

Thermo-mechanical analysis of microcapsules containing phase change materials for cold storage

Item Type	Journal article
Authors	Yu, Qinghua;Al-Duri, Bushra;Tchuenbou-Magaia, Fideline Laure;Zhang, Zhibing;Ding, Yulong;Li, Yongliang
Citation	Yu, Q, Tchuenbou-Magaia, F., Al-Duri, B., Zhang, Z., Ding, Y., & Li, Y. (2018) 'Thermo-mechanical analysis of microcapsules containing phase change materials for cold storage' Applied Energy, 211, pp. 1190-1202. https://doi.org/10.1016/j.apenergy.2017.12.021
DOI	10.1016/j.apenergy.2017.12.021
Publisher	Elsevier
Journal	Applied Energy
Download date	2026-04-15 16:32:54
License	https://creativecommons.org/licenses/by-nc-nd/4.0/
Link to Item	http://hdl.handle.net/2436/621005

Thermo-mechanical analysis of microcapsules containing phase change materials for cold storage

Qinghua Yu, Fideline Tchuenbou-Magaia, Bushra Al-Duri, Zhibing Zhang, Yulong Ding,
Yongliang Li*

Birmingham Centre for Energy Storage, School of Chemical Engineering, University of
Birmingham, Birmingham B15 2TT, United Kingdom

*Corresponding author. Tel.: +44 (0) 121 414 5135, Email: y.li.1@bham.ac.uk (Y. Li)

Abstract

Microencapsulated phase change material slurries (MEPCMSs) offer a potentially efficient and flexible solution for cryogenic-temperature cold storage. In this paper, the phase change material (PCM) microcapsules prepared to form MEPCMSs for cryogenic-temperature cold storage consist of Dowtherm J (DJ) as core material and melamine formaldehyde (MF) as primary shell material. DJ is an aromatic mixture with diethylbenzene as the main component. Composite shell materials are adopted to avoid cracking by adding aluminium oxide (Al_2O_3) nanoparticles or copper (Cu) coating into/on MF shell. In order to explore the heat transfer behaviour and mechanical stability of the microcapsules during the solidification process of PCM, a thermo-mechanical model is established by taking into account of energy conservation, pressure-dependent solid-liquid equilibria, Lamé's equations and buckling theory. Based on the proposed model, the effects of shell thickness, shell compositions and microcapsule size are therefore studied on the variations of pressure difference, freezing point, and latent heat. The cause of shell deformation is clearly explained and the shell buckling modes are predicted using the model, which agree well with the experimental observations. The critical core/shell size ratios of avoiding buckling are proposed for the microcapsules with different compositions. Simultaneously incorporation of Al_2O_3 nanoparticles and Cu coating into/on MF shell can markedly enhance the resistant to buckling. In addition, special attention is paid to cold energy storage capacity of MEPCMSs, which has considerable superiority compared to packed pebble beds.

Keywords: Phase change materials; Microencapsulation; Solidification; Shell buckling; Cold storage.

Nomenclature

Roman letters

a	shell thickness (m)
c_p	specific heat ($\text{J}\cdot\text{kg}^{-1}\cdot\text{K}^{-1}$)
E	Young's modulus (Pa)
ES	stored energy (J)
f	volumetric fraction
F	Legendre function
g	chemical potential ($\text{kJ}\cdot\text{kg}^{-1}$)
h	enthalpy ($\text{kJ}\cdot\text{kg}^{-1}$)
k_f	foundation modulus (N/m^3)
L	latent heat ($\text{kJ}\cdot\text{kg}^{-1}$)
n	buckling mode number
P	pressure (Pa)
r	radius (m)
s	entropy ($\text{J}\cdot\text{kg}^{-1}\cdot\text{K}^{-1}$)
t	time (s)
T	temperature (K)
u	displacement (m)
V	volume (m^3)

Greek letters

α	thermal expansion coefficient (K^{-1})
β	isothermal compressibility (Pa^{-1})
γ	surface tension ($\text{N}\cdot\text{m}^{-1}$)
δ, μ	Lamé's constant

ε	strain
κ	correction factor
λ	thermal conductivity ($\text{W}\cdot\text{m}^{-1}\cdot\text{K}^{-1}$)
ν	Poisson's ratio
ρ	density ($\text{kg}\cdot\text{m}^{-3}$)
σ	stress (Pa)

Subscripts

0	reference or initial
a	atmospheric
b	buckling
c	shell
cr	critical
e	external surface of shell
eq	equivalent
f	freezing or freezing front
i	shell/PCM interface or PCM
l	liquid
m	microcapsule
r, θ, φ	spherical coordinates system
s	solid

Superscripts

*	holistic
---	----------

1. Introduction

Liquid air energy storage (LAES) and pumped thermal electricity storage (PTES) are two emerging grid scale thermal storage technologies, which are good solutions for the intermittency and instability of electricity from renewable energy sources [1-3]. Cryogenic-temperature cold storage is key to improving the overall performance of LAES and PTES systems [4-6]. At present, the two systems generally utilize packed beds for cryogenic-temperature cold storage. However, packed beds have much room for improvement in energy storage capacity, efficiency and flexibility [7-10]. Microencapsulated phase change material slurries (MEPCMSs) have great potential for dynamic and static cryogenic-temperature cold storage applications as they combine the advantages of phase change materials (PCMs) and liquid sensible energy storage materials, and are both transport media (heat transfer fluids) and thermal storage media. MEPCMSs consist of a carrier liquid and PCM microcapsules with a diameter of $<100\ \mu\text{m}$, in general, small enough to be suspended in a carrier liquid. Such partially melting and solidifying slurries can offer very high energy storage densities and heat transfer rates in charging/discharging processes [11]. The good flowability of the MEPCMSs allows them to be transported through pumping, and thus their flow rate can be easily adjusted to realize the desired stored amount of cold energy and objective temperature. Furthermore, their apparent specific heats at set temperatures can be designed by addition of microcapsules with different melting point core PCM, in order to meet the significant specific heat changes of transcritical/supercritical fluids [12]. Therefore, the MEPCMSs can offer a much more flexible strategy for cold storage, which is extremely difficult to achieve using the conventional packed bed.

The utilisation of MEPCMSs will also have a significant impact on the cryogenic industry such as natural gas liquefaction and cold recovery in re-gasification, and air separation/liquefaction [13, 14]. However, most of the research has been conducted only on

moderate or high temperature MEPCMSs with melting points above $-20\text{ }^{\circ}\text{C}$ [15-18], whereas little research can be found on cryogenic MEPCMSs. Technically, the cryogenic MEPCMSs are more challenging compared to MEPCMSs applied at moderate temperatures due to deformation or fragility of the shell of microcapsules and poor heat transfer under cryogenic conditions. The success of MPCMSs in cryogenic temperature cold storage is dependent on the stability of microcapsules under repeated pumping, cyclic heating and cooling as well as long-term storage. As a result, it is important to understand the thermo-mechanical behaviour of MEPCMs in particular during the PCM solidification process.

Several studies have been devoted to the thermo-mechanical behaviour of encapsulated PCM. A composite of mixed graphite and nitrate salts is considered as a solid sphere of PCM encapsulated in a thick shell of graphite by Lopez *et al.* [19] and the shell was modelled as a closed elastic spherical shell with a mobile internal wall and a non-moving external wall. Based on this model, the effects of the shell Young's modulus on the internal pressure, melting point and latent heat, were examined. Pitié *et al.* [20] extended the model to a shell of silicon carbide (SiC) with a free mobile external wall by incorporating the Lamé equations. The variation of internal pressure due to the volume change during the melting process was analytically calculated based on the extended model with a given volume fraction of melted salts, leading to variations of melting point, enthalpy and stored energy. This indicates that the coated PCM should have a low volumetric expansion causing a lower pressure increase so that the coating SiC shell can avoid cracking. Based on the model, the temperature and pressure evolutions during the melting and solidification processes of copper-encapsulated nitrate spheres were simulated at a constant surrounding temperature by Parrado *et al.* [21]. In the simulations the heat transfer equation was decoupled with the mechanical stress equation. Zhao *et al.* [22] compared the time of the melting/solidification process between metal and non-metal encapsulated PCM particles using numerical simulations of heat transfer regardless

of pressure variation. The above investigations are only based on high-temperature thermal energy storage and thermo-mechanical analysis of millimeter-scale encapsulated PCM particles. Mechanical response and properties of microcapsules near room temperature were also evaluated via experiments by Giro-Paloma *et al.* [23] and Su *et al.* [24], without considering the heat transfer behaviour. However, the thermo-mechanical behaviours of PCM microcapsules have rarely been studied for the purpose of cold storage. In particular, the effects of shell thickness and compositions on the thermo-mechanical behaviours have not been clearly addressed by previous studies.

It should be noted that the PCM solidification processes in cold storage are different from those in heat storage in terms of internal pressure and deformation mechanism of shells [20, 25, 26]. Because of the volume shrinkage of PCM during solidification in cold storage application, the internal pressure of microcapsule decreases while the external pressure is constant [27, 28]. When the external pressure is higher than the internal pressure, the spherical microcapsule shell is only subjected to uniform external pressure. The morphology or deformation of such a pressurised spherical shell is then crucial to its properties, such as optical, electromagnetic and heat transfer. The analytical studies of structural behaviour or buckling of complete spherical/spheroidal shells under external pressure have been widely conducted for various objects, including pressure vessels, spherical honeycombs [29], natural fruits and vegetables [30], spherical viruses [31] and biological cells [32]. Timoshenko *et al.* [33] was first to introduce the formulation and solving approach for pressurised buckling of an empty and complete spherical shell based on the axisymmetric assumption and Rayleigh–Ritz approach. Sato *et al.* [34] conducted comparative studies between the exact and simplified approaches to validate the approximation based on the axisymmetric assumption and Rayleigh–Ritz approach. These works show that the approximate formulations enable sufficiently accurate values of the critical buckling pressure and the corresponding buckling

mode number to be obtained. It can also be inferred from the work of Sato *et al.* [34] that when $r_i k_f / E_c < 10^{-3}$ (r_i is the core radius; k_f is the core foundation modulus; and E_c is the shell Young's modulus), the buckling behaviours of the shell filled with elastic materials is the same as that for the empty shell.

This paper presents a first attempt to understand the thermo-mechanical behaviour of spherical microcapsules containing PCM for cold storage application. The microcapsule fabrication process as well as shell modification is described and the morphologies of microcapsules are observed for mechanical analysis. A thermo-mechanical model is established for a single microcapsule during the PCM solidification process, taking into account energy conservation, pressure variation caused by volume shrinkage, pressure-dependent solid-liquid equilibria, shell elastic deformation and buckling behaviour. As $r_i k_f / E_c < 10^{-5}$ in the present study which will be stated in Section 4, it is reasonable to assume that the buckling theory and the corresponding solving approach for empty complete spherical shells proposed by Timoshenko *et al.* [33] are applicable for the buckling analysis of the shell of PCM microcapsules [34]. On the basis of the model, the influences of shell thickness, shell composition and microcapsule size on the solidification process are studied, including the variations of pressure difference, freezing point, latent heat, solidification period and stored energy. The model is used to predict the critical bulking pressure and buckling mode of microcapsules for specific shell thickness and composition. The predicted buckling mode is then compared with experimental observations to validate the proposed model. The energy storage capacities are also compared between MEPCMSs and typical packed beds in LAES and PTES systems. This study can provide significant references for the design of PCM microcapsules without buckling and with better cold storage performance for MEPCMSs.

2. Microcapsule fabrications and testing

The microcapsule studied in this paper consists of melamine formaldehyde (MF) as shell material and Dowtherm J (DJ) as core PCM. The DJ is an aromatic mixture containing diethylbenzene as the main component with a freezing point of -81°C , which was supplied by Dow Chemical Company, US. MF precondensate was purchased from British Industrial Plastics Ltd., UK. The MF shell microcapsules were fabricated via the in-situ polymerization method [35]. The morphologies of fabricated microcapsules after undergoing thermal cycling test were observed by a cryogenic scanning electron microscopy (Cryo-SEM, FEI Quanta 600 FEG SEM equipped with a Quorum PP2000T Cryo-stage). Fig. 1(a) displays the Cryo-SEM image of the microcapsules with pure MF as shell material. It is observed that most of the microcapsules are broken, which is likely due to high brittleness at cryogenic temperature [36]. In order to avoid cracking, composite shell materials were adopted by adding aluminium oxide (Al_2O_3) nanoparticles into MF or electroless copper (Cu) plating on the surface of the MF shell to improve shell mechanical properties. All chemicals used in the fabrication process of microcapsules were purchased from the Sigma-Aldrich, Inc., UK, unless otherwise specified.

The procedure of adding Al_2O_3 nanoparticles is as follows: The surfaces of Al_2O_3 nanoparticles need to be modified by silane coupling agent KH-570 (Sinopharm Chemical Reagent Co., Ltd., China) prior to its addition to the MF shell [37]. A certain amount of Al_2O_3 nanoparticles were dispersed into $\text{C}_2\text{H}_5\text{OH}$ by rapid agitation for 30 min and ultrasonic vibration for 30 min. KH-570 dissolved in $\text{C}_2\text{H}_5\text{OH}$ was subsequently added into the suspension. After undergoing ultrasonic vibration for 30 min and continuous stirring for 2 h, the reaction mixture was then filtered and rinsed with deionized water several times, and finally dried in a vacuum dryer to obtain the modified Al_2O_3 nanoparticles. A certain amount of modified Al_2O_3 nanoparticles were dispersed into core oil DJ with rapid agitation and

ultrasonic vibration. The other procedures about emulsification and polymerization were similar to the fabrication of the pure MF shell microcapsules [35]. Eventually, most of the Al_2O_3 nanoparticles were embedded into the MF shell [37, 38].

A typical procedure of electroless Cu plating is described as follows: Surface sensitization was first implemented by dispersing the MF or MF/ Al_2O_3 shell microcapsules with clean surfaces in an aqueous solution of SnCl_2 and HCl at 30°C for 15 min. The sensitised MF microcapsules were then cleaned with deionized water and dispersed in a solution of PdCl_2 at 30°C for 15 min to accomplish surface activation. The activated MF microcapsules were then cleaned with deionized water and dispersed in the electroless Cu plating solution to form a Cu coating. The solution comprised CuSO_4 , NaOH, HCHO, $\text{NaKC}_4\text{H}_4\text{O}_6$ and Na_2EDTA (ethylene diamine tetraacetic acid). The pH and temperature of the plating solution were adjusted to about 12 and 30°C , respectively.

The microcapsule with Cu coating is referred to as MF-Cu; the one with both Al_2O_3 nanoparticles in shell and Cu coating is named MF-Cu-Al. The Cryo-SEM images of the MF-Cu and MF-Cu-Al microcapsules are shown in Figs. 1(b) and 1(c), respectively. The images show that buckling has occurred for some of the MF-Cu microcapsules while the MF-Cu-Al microcapsules still keep their spherical shape. The occurrence of buckling is closely related to the mechanical properties of shell materials and the ratio of shell thickness to core radius, which will be discussed in Section 4. The microcapsules that did not crack during thermal cycling were then cut into two by an ultramicrotome (Reichert-Jung Ultracut E) to observe the morphology under the Cryo-SEM. Transmission electron microscope (TEM, JEOL 1200EX) was used to examine shell thickness of the microcapsules. It is also shown in Figs. 1(a-c) that the diameter of the microcapsules is around $10\ \mu\text{m}$. And the particle size measurements indicate that the size distribution of the fabricated microcapsules ranges from $10\ \mu\text{m}$ to $100\ \mu\text{m}$ as shown in Fig. 1(d). The chemical studies were performed on a SEM

(Hitachi TM3030) equipped with an energy-dispersive spectrometer (EDS). The existence of Cu on the surface of the so-called MF-Cu and MF-Cu-Al microcapsules is confirmed by the Cu element peaks in the EDS spectra as shown in Figs. 1(e, f). Similarly, the existence of Al_2O_3 on the surface of the so-called MF-Cu-Al microcapsules is certified by the Al element peak in the EDS spectrum as shown in Fig. 1(f), which indicates that the Al_2O_3 nanoparticles have been successfully integrated into the MF shell.

3. Mathematical Models

3.1. Geometry and initial hypotheses

The geometry of a spherical microcapsule is shown in Fig. 2, including a shell and solid/liquid PCM. The external radius of the microcapsule is labelled r_e . The position of the shell/PCM interface and the solidification front are referred to as r_i and r_f , respectively. These parameters are dependent on time t during solidification process.

The main hypotheses applied in this model concerning the PCM and shell are as follows: (a) the density ρ_l , specific heat c_{pl} , and thermal conductivity λ_l are constant, independent of pressure and temperature for the liquid phase of PCM; (b) the liquid pressure within the shell is uniform; (c) as a result of the micro-size capsule, convection heat transfer inside the shell is negligible; (d) viscous energy dissipation is also neglected; (e) the solid phase of PCM possesses homogeneously constant values of density ρ_s , specific heat c_{ps} and thermal conductivity λ_s ; (f) the solid phase of PCM is deformable along with the shell without effect on the shell deformation; (g) the shell is considered to be a homogeneous, isotropic and exhibiting linear elastic behaviour indicated by Young's modulus, with constant values of density ρ_c , specific heat c_{pc} and thermal conductivity λ_c ; (h) the external surface of the shell is at known and uniform temperature and pressure; (i) the conditions of temperature continuity and heat flux conservation are satisfied at the solidification front; (j) there are

equalities of temperature and pressure at the shell/PCM interface. The spherical symmetry before buckling from above mentioned hypotheses allows reduction of the original three-dimensional problem of transfer to a one-dimensional one [19, 20].

3.2. Expression of pressure variation due to volume shrinkage

During the solidification process, the volume shrinkage of the PCM caused by the density difference between solid and liquid phases at a time t is

$$\Delta V = V_{l0} \left(\frac{\rho_l - \rho_s}{\rho_s} \right) f^*(t) \quad (1)$$

where f^* is the ratio of solidified volume at a time t to the initial volume V_{l0} of liquid PCM, which is referred to as solid fraction.

In view of the spherical symmetry of the studied microcapsule before buckling in a spherical coordinate system (r, θ, φ) , the displacement, strain and stress fields of the shell due to elastic deformation are only dependent on r among the three coordinates. Furthermore, the displacement u only has radial component u_r (i.e. $u = u_r$); the strain only has normal strain components ε_{rr} , $\varepsilon_{\theta\theta}$ and $\varepsilon_{\varphi\varphi}$ with $\varepsilon_{\theta\theta} = \varepsilon_{\varphi\varphi}$; and the stress also only has normal stress components σ_{rr} , $\sigma_{\theta\theta}$ and $\sigma_{\varphi\varphi}$ with $\sigma_{\theta\theta} = \sigma_{\varphi\varphi}$. Therefore, the equilibrium equation without the body force can be simplified as

$$\frac{d\sigma_{rr}}{dr} + \frac{2(\sigma_{rr} - \sigma_{\theta\theta})}{r} = 0. \quad (2)$$

The pressure at the shell/PCM interface is equal to the liquid pressure P , while the pressure at the external surface of the shell is equal to ambient pressure P_a (atmospheric). Thus, the boundary conditions for the elastic deformation of the shell are

$$\sigma_{rr}(r = r_{i0}) = -P, \quad \sigma_{rr}(r = r_{e0}) = -P_a, \quad (3)$$

where r_{i0} and r_{e0} are the initial radii of the internal and external walls of the shell, respectively.

The shell undergoes temperature change ΔT during the PCM solidification process. The thermal stress should be taken into account, which is proportional to the thermal expansion coefficient of the shell material α_c . By combining strain-displacement and stress-strain relations with thermal stress [20], the stress-displacement relations are obtained as

$$\sigma_{rr} = \delta \left(\frac{du}{dr} + \frac{2u}{r} \right) + 2\mu \frac{du}{dr} - (3\delta + 2\mu)\alpha_c \Delta T, \quad (4)$$

$$\sigma_{\theta\theta} = \delta \left(\frac{du}{dr} + \frac{2u}{r} \right) + \frac{2\mu u}{r} - (3\delta + 2\mu)\alpha_c \Delta T, \quad (5)$$

where δ and μ are Lamé's constants related to the Young's modulus E_c and Poisson's ratio ν_c as

$$\delta = \frac{E_c \nu_c}{(1 + \nu_c)(1 - 2\nu_c)}, \quad (6)$$

$$\mu = \frac{E_c}{2(1 + \nu_c)}.$$

Substituting Eqns. (4) and (5) into Eqn. (2), yields the simplified Lamé's equations as

$$\frac{d^2 u}{dr^2} + \frac{2}{r} \frac{du}{dr} - \frac{2u}{r^2} = 0. \quad (7)$$

Solving Eqn. (7) with the boundary conditions in Eqn. (3), yields the elastic description of the system as

$$u(r) = r\alpha_c \Delta T + \frac{1}{r_{e0}^3 - r_{i0}^3} \left[\frac{r_{i0}^3 r_{e0}^3 (P - P_a)}{4r^2 \mu} + \frac{(r_{i0}^3 P - r_{e0}^3 P_a)r}{3\delta + 2\mu} \right], \quad (8)$$

$$\sigma_{rr}(r) = \frac{1}{r_{e0}^3 - r_{i0}^3} \left[-\frac{r_{i0}^3 r_{e0}^3 (P - P_a)}{r^3} + (r_{i0}^3 P - r_{e0}^3 P_a) \right], \quad (9)$$

$$\sigma_{\theta\theta}(r) = \frac{1}{r_{e0}^3 - r_{i0}^3} \left[\frac{r_{i0}^3 r_{e0}^3 (P - P_a)}{2r^3} + (r_{i0}^3 P - r_{e0}^3 P_a) \right]. \quad (10)$$

For $r = r_{i0}$, the volume displacement is written as

$$\Delta V = \frac{4}{3} \pi [(u(r_{i0}) + r_{i0})^3 - r_{i0}^3], \quad (11)$$

From Eqns. (1) and (11), it can be derived that

$$u(r_{i0}) = r_{i0} \left(\sqrt[3]{\frac{\rho_l - \rho_s}{\rho_s} f^*(t) + 1} - 1 \right), \quad (12)$$

Before shell formation in the in-situ polymerization process, the liquid PCMs are dispersed in water as spherical droplets. Due to the surface tension, the internal pressure of the droplet is larger than the external pressure. The internal pressure of the droplet can be calculated according to the Young–Laplace equation. It can be assumed that the initial internal pressure inside microcapsules after shell formation is equal to the internal pressure of the droplet. The initial internal pressure is denoted as P_i . Then the initial displacement at $r = r_{i0}$ before solidification of PCM can be calculated as follows:

$$u_0 = \frac{1}{r_{e0}^3 - r_{i0}^3} \left[\frac{r_{i0}^3 r_{e0}^3 (P_i - P_a)}{4r^2 \mu} + \frac{(r_{i0}^3 P_i - r_{e0}^3 P_a) r}{3\delta + 2\mu} \right]. \quad (13)$$

Therefore, Eqn. (12) can be changed to

$$u(r_{i0}) = r_{i0} \left(\sqrt[3]{\frac{\rho_l - \rho_s}{\rho_s} f^*(t) + 1} - 1 \right) + u_0, \quad (14)$$

and by combining with Eqn. (8) gives

$$P = \frac{2(r_{e0}^3 - r_{i0}^3) E_c \left(\sqrt[3]{(\rho_l - \rho_s) f^*/\rho_s + 1} - (1 + \alpha_c \Delta T) + u_0/r_{i0} \right) + 3r_{e0}^3 (1 - \nu_c) P_a}{r_{i0}^3 (2 - 4\nu_c) + r_{e0}^3 (1 + \nu_c)}. \quad (15)$$

3.3. Expression of freezing point and latent heat dependent on pressure

The liquid-solid phase equilibrium can be considered to exist at the solidification front, making the chemical potential of liquid phase equal to that of solid phase. The chemical potential can be approached by a second order Taylor expansion on the basis of some fundamental thermodynamic relations, which is expressed as [19]

$$g_j(T_f, P) = g_{j0} - s_{j0}(T_f - T_{f0}) + \frac{1}{\rho_{j0}}(P - P_0) - \frac{1}{2} \frac{c_{pj0}}{T_0} (T_f - T_{f0})^2 \quad (16)$$

$$-\frac{1}{2} \frac{\beta_{j0}}{\rho_{j0}} (P - P_0)^2 + \frac{\alpha_{j0}}{\rho_{j0}} (T_f - T_{f0})(P - P_0),$$

where the index $j = l$ or s denotes liquid or solid phase; T_f represents the freezing temperature at the pressure P ; $g_j = g_j(T_{f0}, P_0)$ represents the chemical potential at T_{f0} and P_0 ; T_{f0} is the freezing temperature at P_0 representing reference pressure (atmospheric); s_i is the specific entropy; α_i represents the thermal expansion coefficient; and β_i represents the isothermal compressibility; the subscript 0 refers to (T_{f0}, P_0) conditions.

Applying the liquid-solid equilibrium condition ($g_l = g_s$), the following equation for freezing temperature as a function of pressure is obtained:

$$0 = -(s_{l0} - s_{s0})(T_f - T_{f0}) + \left(\frac{1}{\rho_{l0}} - \frac{1}{\rho_{s0}}\right)(P - P_0) - \frac{1}{2} \left(\frac{c_{pl0} - c_{ps0}}{T_0}\right)(T_f - T_{f0})^2 - \frac{1}{2} \left(\frac{\beta_{l0}}{\rho_{l0}} - \frac{\beta_{s0}}{\rho_{s0}}\right)(P - P_0)^2 + \left(\frac{\alpha_{l0}}{\rho_{l0}} - \frac{\alpha_{s0}}{\rho_{s0}}\right)(T_f - T_{f0})(P - P_0). \quad (17)$$

Then via factorizing by $(T_f - T_{f0})$ for Eqn. (17), the solution is derived as

$$T_f(P) = T_{f0} + \frac{-c + \sqrt{c^2 - 4bd}}{2b}, \quad (18)$$

with

$$b = \frac{1}{2} \left(\frac{c_{pl0} - c_{ps0}}{T_{f0}}\right),$$

$$c = (s_{l0} - s_{s0}) - \left(\frac{\alpha_{l0}}{\rho_{l0}} - \frac{\alpha_{s0}}{\rho_{s0}}\right)(P - P_0), \quad (19)$$

$$d = -\left(\frac{1}{\rho_{l0}} - \frac{1}{\rho_{s0}}\right)(P - P_0) + \frac{1}{2} \left(\frac{\beta_{l0}}{\rho_{l0}} - \frac{\beta_{s0}}{\rho_{s0}}\right)(P - P_0)^2.$$

In a similar way, the variation of latent heat with pressure can be predicted. The enthalpy difference between the liquid and solid phases (i.e. latent heat) at thermodynamic equilibrium ($g_l = g_s$) can be expressed as [19]

$$L_f(T_f, P) = \Delta S_f(T_f, P)T_f. \quad (20)$$

For estimation of entropy variation $\Delta s_f(T_f, P)$, Eqns. (16) allows writing

$$s_j \equiv - \left. \frac{\partial g_j}{\partial T} \right|_P = s_{j0} + \frac{c_{pj0}}{T_0} (T_f - T_{f0}) - \frac{\alpha_{j0}}{\rho_{i0}} (P - P_0), \quad (21)$$

and thus

$$\Delta s_f = (s_{l0} - s_{s0}) + \left(\frac{c_{pl0} - c_{ps0}}{T_{f0}} \right) (T_f - T_{f0}) - \left(\frac{\alpha_{l0}}{\rho_{l0}} - \frac{\alpha_{s0}}{\rho_{s0}} \right) (P - P_0). \quad (22)$$

Values of parameters s_{l0} , s_{s0} , ρ_{l0} , ρ_{s0} , c_{pl0} , c_{ps0} , α_{l0} , α_{s0} , β_{l0} , β_{s0} are usually available in the corresponding thermodynamic data bases. Eqns. (18-20) and (22) account for the variation of freezing temperature and latent heat with pressure.

3.4. Heat transfer modelling for spherical microcapsules

The enthalpy method based on a fixed grid [39] was used to model the PCM solidification process while the temperature was directly solved. According to the hypotheses (a) to (g), energy conservation equation can be written as

$$\frac{\partial \left[(\rho c_p)_{eq} T_i \right]}{\partial t} = \frac{1}{r^2} \frac{\partial}{\partial r} \left(\lambda_{eq} r^2 \frac{\partial T_i}{\partial r} \right) - \frac{\partial (\rho_{eq} \Delta h_f)}{\partial t} \quad \text{for } 0 \leq r \leq r_i, \quad (23)$$

$$\frac{\partial (\rho_c c_{pc} T_c)}{\partial t} = \frac{1}{r^2} \frac{\partial}{\partial r} \left(\lambda_c r^2 \frac{\partial T_c}{\partial r} \right) \quad \text{for } r_i < r \leq r_e,$$

where $(\rho c_p)_{eq}$ is the equivalent heat capacity; T_i denotes the temperature distributions in the PCM layer; λ_{eq} is the equivalent thermal conductivity; ρ_{eq} is the equivalent density; Δh_f represents the solidification enthalpy which can be defined as a product of latent heat L_f and local liquid fraction f_l , i.e. $\Delta h_f = f_l L_f$; and T_c is the temperature distributions in the shell layer. $(\rho c_p)_{eq}$, ρ_{eq} and λ_{eq} are given by

$$(\rho c_p)_{eq} = \rho_l c_{pl} f_l + \rho_s c_{ps} (1 - f_l), \quad (24)$$

$$\rho_{eq} = \rho_l f_l + \rho_s (1 - f_l),$$

$$\lambda_{eq} = \lambda_l f_l + \lambda_s (1 - f_l).$$

For the pure PCM with a fixed freezing point, the relationship between local liquid fraction and temperature can be described as

$$f_l(r, t) = \begin{cases} 1, & T_p \geq T_f \\ 0, & T_p < T_f \end{cases} \quad (25)$$

Boundary conditions of the problem are

$$\begin{aligned} -\lambda_{eq} \frac{\partial T_i}{\partial r} &= 0 \text{ at } r = 0, \\ \lambda_{eq} \frac{\partial T_i}{\partial r} &= \lambda_c \frac{\partial T_c}{\partial r}, \text{ and } T_i = T_c \text{ at } r = r_i, \end{aligned} \quad (26)$$

$$T_c = T_e(t) \text{ at } r = r_e,$$

where $T_e(t)$ is the temperature at the external surface of shell. Initially, $T_i(r, 0) = T_c(r, 0) = T_0$, which is uniform. For the integration of the phase change into pressure variation in Eqn. (15), an expression calculating $f^*(t)$ is required, which can be written as:

$$f^*(t) = 1 - \frac{3}{r_{i0}^3} \int_0^{r_i} r^2 f_l(r, t) dr. \quad (27)$$

The total energy stored within the microcapsule during solidification mainly consists of latent energy and sensible energy, which can be expressed as

$$ES(f^*) = \int_0^{f^*} \rho_l V_{l0} L_f d\vartheta + \int_{T(f^*=0)}^{T(f^*)} V_{l0} [\rho_l c_{pl} f_l + \rho_s c_{ps} (1 - f_l)] d\vartheta. \quad (28)$$

3.5. Buckling of uniform pressurised spherical shells

If a spherical shell is subjected to uniform external pressure, it may retain its spherical form and undergo only a uniform compression with radial displacement. The magnitude of the uniform compressive stress in this case can be calculated by Eqns. (9) and (10). If the pressure increases beyond a certain limit, the spherical equilibrium form of the compressed shell may become unstable and buckling occurs [33]. As described before, the axisymmetric assumption has little effect on the calculated values of the critical buckling pressure and the

corresponding buckling mode number [34]. Thus, it is assumed that the buckling deformation is axisymmetric with respect to the vertical axis in order to simplify the calculation of the critical pressure. Considering the discrepancy between theory and experiment existing during buckling of spherical shell under uniform external pressure [33, 40], the actual critical buckling pressure can be obtained by modifying the theoretical expression, which is as follows [33]:

$$P_{cr} = \kappa \frac{2E_c a^2}{r_i^2 \sqrt{3(1-\nu_c^2)}} \quad (29)$$

where a is the shell thickness and κ is the correction factor which equals about 0.7 [41].

Because of axisymmetric buckling, the small displacements of the shell during bulking from the compressed spherical form only have the components $u_{b\theta}$ and u_{br} , respectively, in meridian and radial directions θ and r . The two components are calculated by [33]:

$$u_{b\theta} = \sum_{m=1}^{\infty} A_n \frac{dF_n(\cos \theta)}{d\theta} \quad (30)$$

$$u_{br} = \sum_{n=1}^{\infty} B_n F_n(\cos \theta)$$

where $F_n(\cos \theta)$ is Legendre functions; A_n, B_n can be obtained by solving

$$A_n[m_n + (1 + \nu_c) + \phi] + B_n[\omega m_n + (1 + \nu_c) + \phi] = 0,$$

$$A_n[\omega m_n^2 + (1 + \nu_c)(m_n + 2) + \phi(m_n + 2)] \quad (31)$$

$$+ B_n[\omega m_n^2 + (3 + \nu_c)\omega m_n + 2(1 + \nu_c) - \phi(m_n - 2)] = 0,$$

where $\omega = a^2/(12r_i^2)$; $m_n = n(n + 1) - 2$; n is an integer representing the buckling mode number. The relation between ϕ and m_n is as follows [33]:

$$\phi = \frac{(1 - \nu_c^2) + \omega[m_n^2 + 2m_n + (1 + \nu_c)^2]}{m_n + (1 + 3\nu_c)} \quad (32)$$

According to equation (32), n is selected to obtain the smallest value of ϕ where buckling may occur.

4. Results and discussions

Heat transfer and mechanical behaviour of the microcapsule during PCM solidification are simulated using validated models in Section 3. The temperature at the external surface of the microcapsule is decreasing as the microcapsules flow with the slurry in a heat exchanger for the charging process of cold energy. It is thus assumed that the temperature at the external surface of the microcapsule decreases from -80°C to -85°C at a cooling rate of $5^{\circ}\text{C}/\text{min}$ over the freezing point of -81°C in the simulations. The external pressure of microcapsule is constant and equal to atmospheric pressure (≈ 0.1 MPa). As mentioned in Section 3.2, the initial internal pressure calculated according to the Young–Laplace equation equals about 0.11 MPa for the microcapsule with $r_i = 5$ μm .

The thermodynamic properties of PCM (DJ) at atmospheric pressure P_0 are listed in Table 1 [42]. The theoretical properties of pure MF are supplied in Table 2 for reference [43]. It should be noted that the actual properties of the fabricated shell depend on the actual polymerization effect. Thus they are variable and different from the theoretical values, especially for the Young's modulus. The research of Giro-Paloma *et al.* [23] manifests that the effective Young's modulus E_m of primordial microcapsules with pure MF as shell is subject to approximately normal random distribution with an average value of 30 MPa. The value of E_m has a linear relationship with the actual Young's modulus of the shell E_c , which is $E_m = 0.16aE_c/(r_i + a)$ [44]. The calculated average value of E_c for MF shell is therefore about 0.6 GPa according to the values of r_i and a [23]. As described in Section 2, the shell is made of composite materials of MF and Cu or Al_2O_3 . The compositions of MF-Cu shell are specified as 95% MF and 5% Cu by volume while those of MF-Cu-Al shell are specified as 90% MF, 5% Al_2O_3 and 5% Cu by volume. It is estimated by weighted average that E_c is around 1.0 GPa for MF-Cu shell and around 3.0 GPa for MF-Cu-Al shell. The Poisson's

ratios for the three kinds of compositions are all between 0.2 and 0.4 and the value in this range has little effect on the results. The Poisson's ratio of the composite materials is thus assumed to be 0.3. The estimated Young's modulus can be used as a characteristic value to represent the property changes caused by compositions for comparative analysis.

4.1. Validation of the model

In order to validate the proposed model, the results calculated based on the model established in this paper were compared with those in literature [19, 39] for the same problems and properties. Figs. 3(a, b) compare the temperature profile at $t = 500$ s and solidification rate in terms of liquid fraction for a square cavity containing PCM between the present study and the literature [39]. Results from both this study and literature are similar, suggesting that the heat transfer model for phase change based on the enthalpy method in Section 3.4 is reliable. Figs. 3(c, d) compare the variations of internal pressure, melting temperature and latent heat during melting coupled with heat transfer for salt particles coated in a graphite matrix between the current study and literature [19]. The results obtained in this study show a satisfactory agreement with the literature, indicating that the pressure variation model in Section 3.2 and pressure-dependent dynamic equilibrium model in Section 3.3 together with the heat transfer model in Section 3.4 are sufficiently accurate. Comparison of the predicted results with experimental results in Section 4.5 also validates the buckling models in Section 3.5.

4.2. Effects of shell thickness

The effects of shell thickness are analyzed for MF-Cu microcapsules with $r_i = 5 \mu\text{m}$ in this section. Fig. 4(a) illustrates the evolutions of differences between external and internal pressures under different shell thicknesses during the solidification process ($f^*: 0 \rightarrow 1$). The internal pressure is calculated from Eqn. (15). As a consequence of PCM volume shrinkage,

the internal pressure will be progressively decreased until zero and thus the pressure difference will be progressively increased until 0.1 MPa. The increasing rate of pressure difference decreases with the increase of r_i/a . The critical pressures calculated by Eqn. (29) are traced to compare the progress of the pressure differences to the buckling limits of the shells. Buckling occurs only when the pressure difference increases to the critical pressure. The position as buckling occurs is marked according to the critical pressure represented by horizontal line in the figure. Shell bulking will not occur for $r_i/a = 20$ or 50 , while shell bulking will occur for $r_i/a = 100$ or 120 . This accounts for the phenomenon that buckling occurs for some of the MF-Cu microcapsules in Fig 1(b). Compared with the case where $r_i/a = 100$, the solid fraction as bulking occurs for $r_i/a = 120$ is smaller because the critical pressure is lower, although the pressure difference increases more slowly. The above results imply that reducing shell thickness leads to shell buckling or makes buckling occur at the earlier solidification stage. The buckling limit indicates that it becomes impossible to consider the heat transfer behaviour of PCM based on the mentioned approach when the pressure difference is beyond the critical pressure. In order to compare the different shell thicknesses and compositions, the following Figs. 4(b-d) and 5 still consider up to 100% of solidified PCM without buckling.

The freezing point variations ($T_f - T_{f0}$) calculated from Eqn. (18) at different solidification stages are shown in Fig. 4(b). It can be found that the freezing point slightly decreases until a constant value is reached according to zero internal pressure as the solidification process carries on. The coated PCM will no longer solidify at constant temperature before the internal pressure decreases to zero. The decreasing rate of freezing point dependent on the internal pressure decreases with the increase of r_i/a . The lowest freezing point before shell buckling for $r_i/a = 100$ is lower than that for $r_i/a = 120$. Fig. 4(c) shows the latent heat variations ($L_f - L_{f0}$) calculated from Eqn. (20) at different

solidification stages. As both the internal pressure and freezing point decrease, the latent heat slightly increases. The increase of r_i/a slows the increase of latent heat in the solidification process.

Fig. 4(d) illustrates the solidification time of PCM obtained by solving Eqn. (23) under different shell thicknesses. The thickness has little influence on the total solidification period of PCM at a shell thermal conductivity of $0.5 \text{ W}\cdot\text{m}^{-1}\cdot\text{K}^{-1}$. The effects of shell thicknesses with different thermal conductivities on the solidification time of PCM are shown in Fig. 5. For $r_i/a = 100$, the thermal conductivity of shell has nearly no influence on the PCM solidification period. For $r_i/a = 20$, the solidification period of PCM increases with the decrease in the thermal conductivity of the shell. The difference in the solidification period between $r_i/a = 20$ and 100 also increases with the decrease of the thermal conductivity of the shell. This implies that the shell thickness has considerable effect on the solidification time and its increase extends the solidification period of PCM when the shell has low thermal conductivity. This suggests that the shell thickness affects the heat transfer behaviour of MEPCMSs via influencing the solidification time inside microcapsules.

4.3. Effects of shell compositions

Comparative analysis is carried out among MF, MF-Cu and MF-Cu-Al microcapsules with $r_i = 5 \text{ }\mu\text{m}$ and $r_i/a = 100$. The differences of shell compositions are reflected in the differences in the Young's moduli as described above. Fig. 6(a) displays the evolution of differences between external and internal pressures with solidification of PCM under different shell compositions. Among the three kinds of microcapsules, the MF-Cu-Al microcapsule with highest Young's modulus has fastest increasing rate of pressure difference. The pressure differences for the MF and MF-Cu microcapsules reach the critical buckling pressures at $f^* = 0.56$ and at $f^* = 0.52$, respectively. As a result, shell buckling occurs at the corresponding positions for the two microcapsules. Compared with the MF microcapsule, the

MF-Cu microcapsule buckles at an earlier solidification stage because of a higher rate of increase in the pressure difference, although it has a higher critical pressure. Because the MF-Cu-Al microcapsule possesses higher critical buckling pressure, the shell buckling does not take place during solidification. This implies that the increase of Young's modulus augments the critical pressure and therefore avoids shell buckling. The reason why there are different morphologies between the MF-Cu and MF-Cu-Al microcapsules in Figs. 1(b, c) can easily be obtained from the above analysis. The calculation analysis and experimental test indicate that using composite shell to elevate the Young's modulus is a feasible method to avoid buckling.

As shown in Fig. 6(b), the MF-Cu-Al microcapsule has the lowest freezing point at the same solidification stage among the three types of microcapsules before their freezing points become constant, which is determined by its internal pressure. The lowered freezing point will slow down the solidification process. The freezing point persistently decreases during the whole solidification process for the MF microcapsule, rather than remaining constant at the later solidification stage similar to the situation of other microcapsules. Fig. 6(c) indicates that the MF-Cu-Al microcapsule exhibits the highest average value of latent heat among the three types of microcapsules. This results in an increase of cold energy stored by releasing latent heat. Fig. 6(d) shows that the shell compositions have a slight effect on the solidification time. The MF-Cu-Al microcapsule exhibits the slowest solidification process, which coincides with the situation of freezing point as shown in Fig. 6(b).

4.4. Effects of microcapsule size

The solidification processes are comparatively analysed for the MF-Cu-Al microcapsules with different sizes at $r_i/a = 100$. It is obvious that the solidification period of PCM increases as the microcapsule size increases. The exact solidification periods for microcapsules with different sizes are shown in Fig. 7(a). The solidification periods for microcapsules with $r_i = 5, 25$ and 50 are 0.5 s, 2.1 s and 4.5 s, respectively. The solidification

period will directly influence the charging efficiency of cold energy. In addition, the starting time for solidification is independent of the microcapsule size. The stored energy calculated by Eqn. (28) is also examined for microcapsules with different sizes at the same r_i/a as shown in Figs. 7(b, c). The stored latent energy increases linearly regardless of microcapsule size, while the stored sensible energy is nearly constant because of the narrow temperature changes during the solidification process.

4.5. Critical pressure and buckling mode

According to the buckling theory, the condition for shell buckling is that the difference between external and internal pressures should be greater than the critical buckling pressure. The external pressure is atmospheric pressure and the minimum internal pressure is zero, so that the maximum pressure difference is atmospheric pressure for the microcapsules. For prescribed shell materials or compositions, the critical buckling pressure is only dependent on r_i/a in accordance with Eq. (29). Fig. 8(a) depicts the variation of critical buckling pressure with respect to r_i/a for the MF, MF-Cu and MF-Cu-Al shells. The figure shows that the critical pressure decreases with an increase in r_i/a and the MF-Cu-Al shell has highest critical pressure among the three shells at the same r_i/a . When $r_i/a \geq 72, 92$ and 160 for the MF, MF-Cu and MF-Cu-Al shells respectively, the critical pressure decreases below atmospheric pressure (≈ 0.1 MPa), indicating that the pressure differences will exceed the critical pressure at a certain solidification stage and buckling will thus occur. Thus, the conditions for avoiding buckling during the solidification process for MF, MF-Cu and MF-Cu-Al shells are $r_i/a < 72, 92$ and 160 , respectively. This implies that the MF-Cu microcapsule is easier to buckle than the MF-Cu-Al one, which explains the morphology difference between the two kinds of microcapsules as shown in Figs 1(b, c).

As shown in Fig. 8(b), the buckling mode number obtained by solving Eqn. (32) increases with r_i/a and coincides with the calculation of Sato *et al.* [34]. This suggests that

the microcapsules present different buckling modes at different r_i/a , because they are corresponding to the mode numbers. Figs. 9(a, b) demonstrate the buckling modes of MF-Cu microcapsules calculated from Eqn. (30) at $r_i/a = 140$ and 14, of which the mode numbers are 23 and 6, respectively. The buckling waves on one side of symmetry axis are labeled with numbers. The buckling deformation is asymmetric about the equator for the odd mode number as shown in Fig. 9(a), whilst it is symmetric about the equator for the even mode number as shown in Fig. 9(b).

Fig. 9(c) displays the cross-sectional Cryo-SEM image of a buckled MF-Cu microcapsule obtained experimentally. The buckling on one side of the axis of symmetry vanished when the microcapsules were cut. The calculated buckling deformation and mode number at $r_i/a = 140$ as shown in Fig. 9(a) agree well with the image observed experimentally as shown in Fig. 9(c). The condition for buckling is satisfied for the MF-Cu microcapsule of $r_i/a = 140$, which means that the prediction about buckling is reasonable. From the Cryo-SEM image in Fig. 9(c) the shell thickness cannot be obtained, but it can be derived from the value of r_i/a in Fig. 9(a). The resulting shell thickness is about 36 nm.

The cross-sectional TEM image of a buckled MF-Cu microcapsule obtained through experiments is shown in Fig. 9(d). It can be observed from this figure that the microcapsule diameter is around 11 μm and the shell thickness is 386 nm. The value of r_i/a for the microcapsule in Fig. 9(d) is about 14, which is the same as that in Fig. 9 (b). By Comparing Figs. 9(b) and 9(d), it is easily found that the predicted buckling deformation and mode number are highly consistent with the experimental observations at the same r_i/a . This further confirms the validity of the proposed buckling model in Section 3.5. It should be pointed out that the buckling condition for a microcapsule of $r_i/a = 14$ under atmospheric pressure is $E \leq 23$ MPa, which is smaller than the adopted value of E for the MF-Cu microcapsule above. It can be inferred that the small value of E is a consequence of a poor quality of polymerization and electroless plating, which is likely to randomly occur during

the fabrication process of microcapsules.

4.6. Energy storage capacity of MEPCMSs

A cold storage unit is the essential component for the PTES system [7, 45] and can also be applied to improve the round trip efficiency of the LAES system [8, 46]. Both McTigue *et al.* [7] and Sciacovelli *et al.* [8] used a packed bed as the cold storage unit for the PTES and LAES systems, respectively. In the packed bed, the storage medium is spherical pebbles made of Fe_3O_4 with an average void fraction of 0.35 for the PTES system, while it is spherical quartzite rocks with an average void fraction of 0.38 for the LAES system. In this study, it is attempted to use a tank containing MEPCMS as the cold storage unit instead of the packed bed in the cryogenic temperature region. The selected MEPCMS consists of a carrier liquid and the DJ microcapsules with an assumed volumetric concentration of 20%. Because the working temperature regions in the cold storage units of the two systems are different, the R22 and propane are adopted as the carrier liquid for PTES and LAES systems, respectively. The thermophysical properties of R22 and propane come from the commercial software REFPROP 8.0 developed by National Institute of Standards and Technology (NIST). The equivalent thermophysical properties of MEPCMSs were calculated by the method shown in [47].

Table 3 compares the energy storage capacity between the typical packed beds and the selected MEPCMSs at the same pressure and temperature conditions for the PTES and LAES systems, respectively. The calculation of energy storage density only considered the static energy balance of heat transfer. For the PTES system, the mass-based energy storage density of the MEPCMS is about 2.4 times that of the packed bed and the volume-based energy storage density of the MEPCMS is 5.2 MJ/m^3 greater than that of the packed bed. For the LAES system, the MEPCMS has about 3.8 times the mass-based energy storage density and around 1.8 times the volume-based energy storage density of the packed bed. Because of a temperature gradient existing along the packed bed in actual applications, not all of the cold

storage medium can be fully utilized [48, 49]. Therefore, the difference in the energy storage density between the MEPCMS and packed bed will be further enlarged in actual applications. In view of its higher energy storage capacity, using the MEPCMS as a cold storage medium can result in more compact PTES and LAES systems.

5. Conclusions

A numerical model was established to describe the thermo-mechanical behavior of spherical microcapsules containing PCM for cryogenic-temperature cold storage. The model combines energy conservation equations, pressure-dependent solid-liquid equilibria, Lamé's equations and buckling theory. During the charging process of cold energy, the PCM solidification results in volume shrinkage and the pressure inside the microcapsule thus decreases. The main consequences of this depressurisation are a progressive augmentation of the difference between external and internal pressures, a progressive diminution of freezing point of the PCM and a progressive increase of its latent heat. When the pressure difference increases to the critical buckling pressure, shell buckling will occur.

The influences of shell thickness and compositions on the thermo-mechanical behaviour of a microcapsule during the PCM solidification process were studied on the basis of the developed model. The decrease of shell thickness slows down the decrease of internal pressure, and thus diminishes the changing rates of freezing point and latent heat. The shell thickness has little effect on the solidification time of PCM when the shell material has a high thermal conductivity. When the critical pressure reduces below 0.1 MPa with the decrease in shell thickness at the same core radius, shell buckling will occur during the solidification process of PCM; Further decreasing shell thickness leads to the occurrence of shell buckling at an earlier solidification stage. The Young's modulus of the shell is increased by embedding Al_2O_3 nanoparticles into or electroless Cu plating on the surface of MF the shell. The increase

in the Young's modulus of the shell speeds up the variations of internal pressure, freezing point and latent heat and thus leads to a slower solidification process, while enhancing the resistance to buckling. The conditions for avoiding buckling during the solidification process for MF, MF-Cu and MF-Cu-Al shells are that the ratio of core radius to shell thickness is less than 72, 92 and 160, respectively. The buckling mode predicted by the thermo-mechanical model is highly consistent with the experimental observations and the mode number increases with the ratio of core radius to shell thickness. The model can be applied to predict the conditions of avoiding shell buckling as well as the shell thickness or Young's modulus based on observed buckling mode.

The shell buckling and solidification time of PCM microcapsules are crucial to the heat transfer behavior of MEPCMSs and charging efficiency of cold energy. The comparative analysis indicates that MEPCMSs have higher cold energy storage capacity than packed pebble beds in PTES and LAES systems. The present study can provide significant guidance for precisely tailoring the key parameters of PCM microcapsules to enable successful and high-efficiency applications of MEPCMSs for cold storage.

Acknowledgement

The authors gratefully acknowledge the financial support of the Engineering and Physical Sciences Research Council (EPSRC) of the United Kingdom under grants EP/N000714/1 and EP/N021142/1.

References

- [1] Guizzi GL, Manno M, Tolomei LM, Vitali RM. Thermodynamic analysis of a liquid air energy storage system. *Energy* 2015;93:1639-47.
- [2] Peng H, Shan X, Yang Y, Ling X. A study on performance of a liquid air energy storage system with packed bed units. *Appl Energy* 2018;211:126-35.
- [3] Thess A. Thermodynamic Efficiency of Pumped Heat Electricity Storage. *Phys Rev Lett* 2013;111:110602.
- [4] Morgan R, Nelmes S, Gibson E, Brett G. Liquid air energy storage – Analysis and first results from a pilot scale demonstration plant. *Appl Energy* 2015;137:845-53.
- [5] She X, Peng X, Nie B, Leng G, Zhang X, Weng L, et al. Enhancement of round trip efficiency of liquid air energy storage through effective utilization of heat of compression. *Appl Energy* 2017;206:1632-42.
- [6] White A, Parks G, Markides CN. Thermodynamic analysis of pumped thermal electricity storage. *Appl Therm Eng* 2013;53:291-8.
- [7] McTigue JD, White AJ, Markides CN. Parametric studies and optimisation of pumped thermal electricity storage. *Appl Energy* 2015;137:800-11.
- [8] Sciacovelli A, Vecchi A, Ding YL. Liquid air energy storage (LAES) with packed bed cold thermal storage – From component to system level performance through dynamic modelling. *Appl Energy* 2017;190:84-98.
- [9] Peng H, Li R, Ling X, Dong H. Modeling on heat storage performance of compressed air in a packed bed system. *Appl Energy* 2015;160:1-9.
- [10] Peng H, Yang Y, Li R, Ling X. Thermodynamic analysis of an improved adiabatic compressed air energy storage system. *Appl Energy* 2016;183:1361-73.
- [11] Ma X, Omer SA, Riffat SB, Zhang W. Investigation of energy transportation capability of a phase change slurry through a cold storage-cooling coil system. *Int J Energy Res* 2009;33:999-1004.
- [12] Griffiths PW, Eames PC. Performance of chilled ceiling panels using phase change material slurries as the heat transport medium. *Appl Therm Eng* 2007;27:1756-60.

- [13] Chiu C-H. Commercial and technical considerations in the development of offshore liquefaction plant. 23rd World Gas Conference. Amsterdam, Netherlands; 2006. p. 2485-96.
- [14] Li Y, Wang X, Ding Y. An optimal design methodology for large-scale gas liquefaction. *Appl Energy* 2012;99:484-90.
- [15] Delgado M, Lázaro A, Mazo J, Zalba B. Review on phase change material emulsions and microencapsulated phase change material slurries: Materials, heat transfer studies and applications. *Renew Sust Energ Rev* 2012;16:253-73.
- [16] Qiu Z, Ma X, Zhao X, Li P, Ali S. Experimental investigation of the energy performance of a novel Micro-encapsulated Phase Change Material (MPCM) slurry based PV/T system. *Appl Energy* 2016;165:260-71.
- [17] Wang T, Wang S, Luo R, Zhu C, Akiyama T, Zhang Z. Microencapsulation of phase change materials with binary cores and calcium carbonate shell for thermal energy storage. *Appl Energy* 2016;171:113-9.
- [18] Alva G, Huang X, Liu L, Fang G. Synthesis and characterization of microencapsulated myristic acid–palmitic acid eutectic mixture as phase change material for thermal energy storage. *Appl Energy* 2017;203:677-85.
- [19] Lopez J, Caceres G, Palomo Del Barrio E, Jomaa W. Confined melting in deformable porous media: A first attempt to explain the graphite/salt composites behaviour. *Int J Heat Mass Transf* 2010;53:1195-207.
- [20] Pitié F, Zhao CY, Caceres G. Thermo-mechanical analysis of ceramic encapsulated phase-change-material (PCM) particles. *Energy Environ Sci* 2011;4:2117-24.
- [21] Parrado C, Cáceres G, Bize F, Bubnovich V, Baeyens J, Degrève J, et al. Thermo-mechanical analysis of copper-encapsulated $\text{NaNO}_3\text{--KNO}_3$. *Chem Eng Res Des* 2015;93:224-31.
- [22] Zhao W, Neti S, Oztekin A. Heat transfer analysis of encapsulated phase change materials. *Appl Therm Eng* 2013;50:143-51.
- [23] Giro-Paloma J, Barreneche C, Martínez M, Šumiga B, Fernández AI, Cabeza LF. Mechanical response evaluation of microcapsules from different slurries. *Renew Energy* 2016;85:732-9.

- [24] Su J-F, Wang X-Y, Dong H. Micromechanical properties of melamine–formaldehyde microcapsules by nanoindentation: Effect of size and shell thickness. *Mater Lett* 2012;89:1-4.
- [25] Alam TE, Dhau JS, Goswami DY, Stefanakos E. Macroencapsulation and characterization of phase change materials for latent heat thermal energy storage systems. *Appl Energy* 2015;154:92-101.
- [26] Lashgari S, Arabi H, Mahdavian AR, Ambrogi V. Thermal and morphological studies on novel PCM microcapsules containing n-hexadecane as the core in a flexible shell. *Appl Energy* 2017;190:612-22.
- [27] Liu M-J, Fan L-W, Zhu Z-Q, Feng B, Zhang H-C, Zeng Y. A volume-shrinkage-based method for quantifying the inward solidification heat transfer of a phase change material filled in spherical capsules. *Appl Therm Eng* 2016;108:1200-5.
- [28] Assis E, Ziskind G, Letan R. Numerical and experimental study of solidification in a spherical shell. *J Heat Transf* 2009;131:024502.
- [29] Tarnai T. Buckling patterns of shells and spherical honeycomb structures. *Comput Math Appl* 1989;17:639-52.
- [30] Yin J, Cao Z, Li C, Sheinman I, Chen X. Stress-driven buckling patterns in spheroidal core/shell structures. *Proceedings of the National Academy of Sciences* 2008;105:19132-5.
- [31] Ru CQ. Buckling of empty spherical viruses under external pressure. *J Appl Phys* 2009;105:124701.
- [32] Vliegenthart GA, Gommer G. Compression, crumpling and collapse of spherical shells and capsules. *New J Phys* 2011;13:045020.
- [33] Timoshenko SP, Gere JM. *Theory of elastic stability*: McGraw-Hill; 1961.
- [34] Sato M, Wadee MA, Iiboshi K, Sekizawa T, Shima H. Buckling patterns of complete spherical shells filled with an elastic medium under external pressure. *Int J Mech Sci* 2012;59:22-30.
- [35] ACM Comput. Surv. Long Y, York D, Zhang Z, Preece JA. Microcapsules with low content of formaldehyde: preparation and characterization. *J Mater Chem* 2009;19:6882-7.

- [36] Hechtel K. Design considerations for the use of plastic materials in cryogenic environments. Curbell Plastics, Inc.; 2014. <https://www.curbellplastics.com/Research-Solutions/Technical-Resources/Technical-Resources/Plastic-Materials-in-Cryogenic-Environments>.
- [37] Jiang X, Luo R, Peng F, Fang Y, Akiyama T, Wang S. Synthesis, characterization and thermal properties of paraffin microcapsules modified with nano- Al_2O_3 . *Appl Energy* 2015;137:731-7.
- [38] Niu X-W, Sun Y-M, Ding S-N, Chen C-C, Song B, Xu H-B, et al. Synthesis of enhanced urea-formaldehyde resin microcapsules doped with nanotitania. *J Appl Polym Sci* 2012;124:248-56.
- [39] Voller VR, Cross M, Markatos NC. An enthalpy method for convection/diffusion phase change. *Int J Numer Methods Eng* 1987;24:271-84.
- [40] Kármán TV, Tsien HS. The buckling of spherical shells by external pressure. *J Aeronautical Sci* 1939;7:43-50.
- [41] Pan B, Cui W. An overview of buckling and ultimate strength of spherical pressure hull under external pressure. *Mar Struct* 2010;23:227-40.
- [42] Dowtherm J heat transfer fluid: Product technical data. The Dow Chemical Company; 1997. <http://www.dow.com/heattrans/>.
- [43] Harper CA. *Modern Plastics Handbook*. New York: McGraw-Hill; 1999.
- [44] Liu M. Understanding the mechanical strength of microcapsules and their adhesion on fabric surfaces [Doctoral Dissertation]. United Kingdom: University of Birmingham; 2010.
- [45] Frate GF, Antonelli M, Desideri U. A novel Pumped Thermal Electricity Storage (PTES) system with thermal integration. *Appl Therm Eng* 2017;121:1051-8.
- [46] Li Y, Cao H, Wang S, Jin Y, Li D, Wang X, et al. Load shifting of nuclear power plants using cryogenic energy storage technology. *Appl Energy* 2014;113:1710-6.
- [47] Zeng R, Wang X, Chen B, Zhang Y, Niu J, Wang X, et al. Heat transfer characteristics of microencapsulated phase change material slurry in laminar flow under constant heat flux. *Appl Energy* 2009;86:2661-70.
- [48] Araki H, Nakabaru M, Chino K. Simulation of heat transfer in the cool storage unit of a liquid-air energy storage system. *Heat Transf—Asian Res* 2002;31:284-96.

[49] Chai L, Liu J, Wang L, Yue L, Yang L, Sheng Y, et al. Cryogenic energy storage characteristics of a packed bed at different pressures. *Appl Therm Eng* 2014;63:439-46.

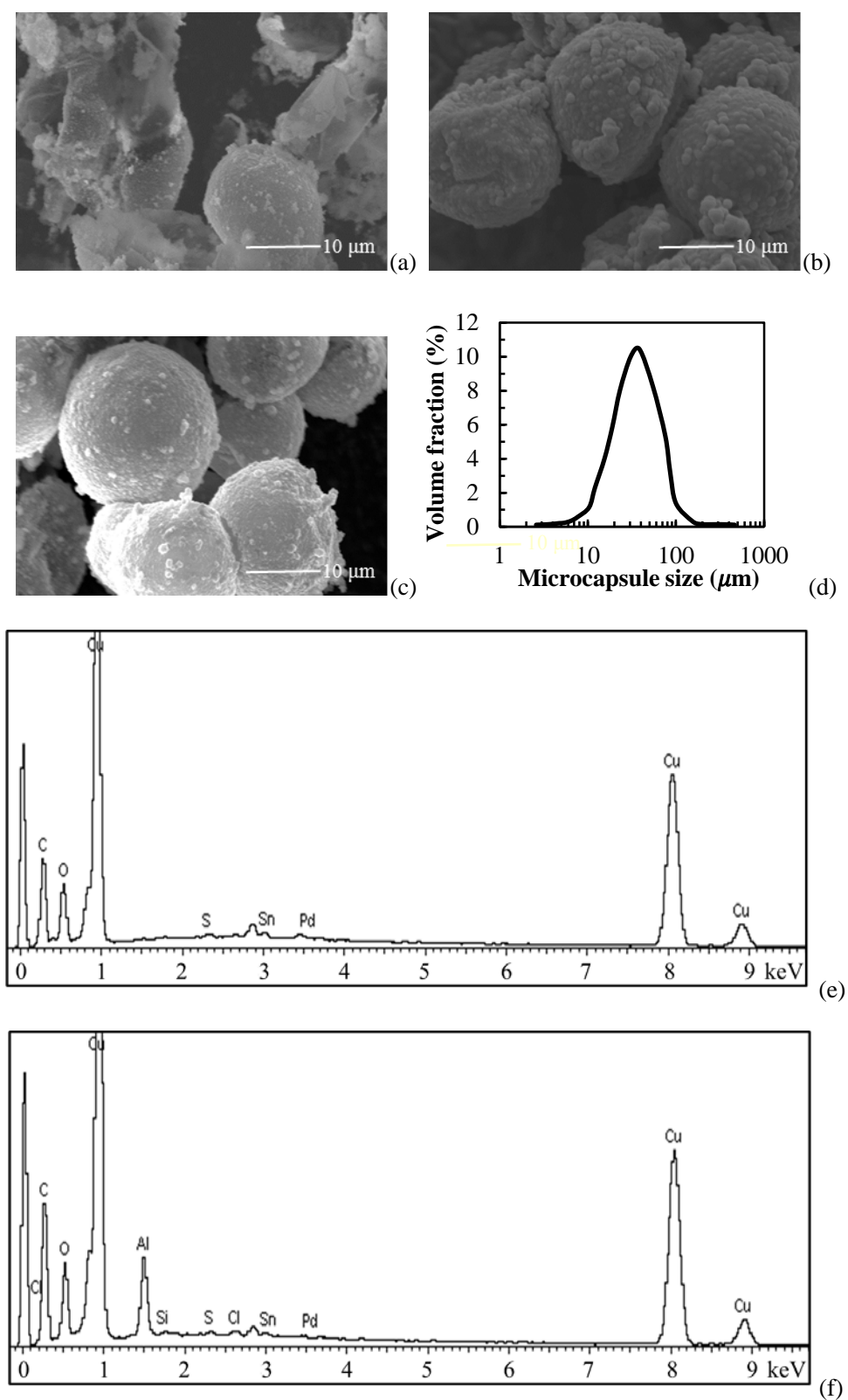


Fig. 1 Microcapsules: (a,b,c) Cryo-SEM images of MF, MF-Cu and MF-Cu-Al microcapsules; (d) Size distribution; (e,f) EDS spectra of MF-Cu and MF-Cu-Al microcapsules.

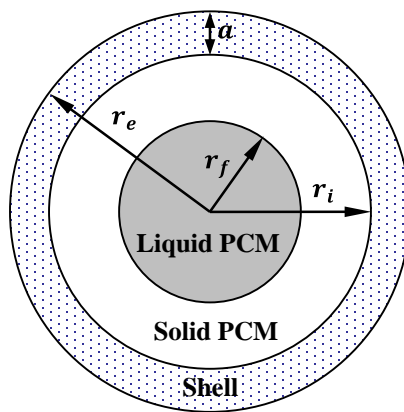
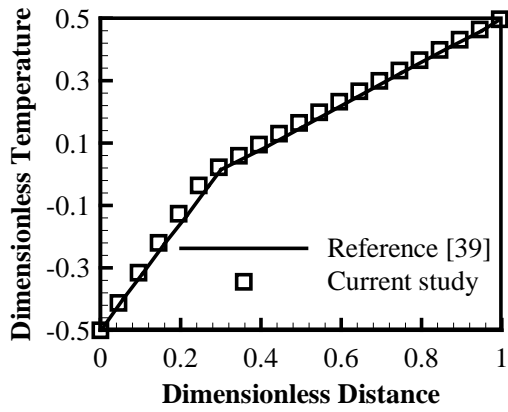
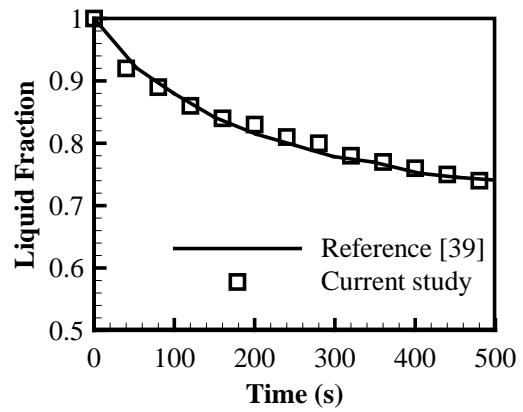


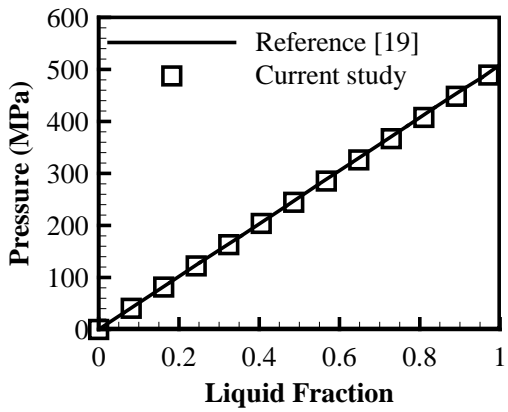
Fig. 2 Geometry of the spherical microcapsule containing PCM.



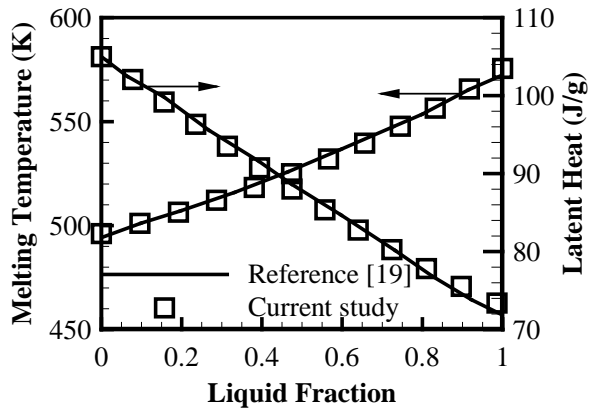
(a)



(b)

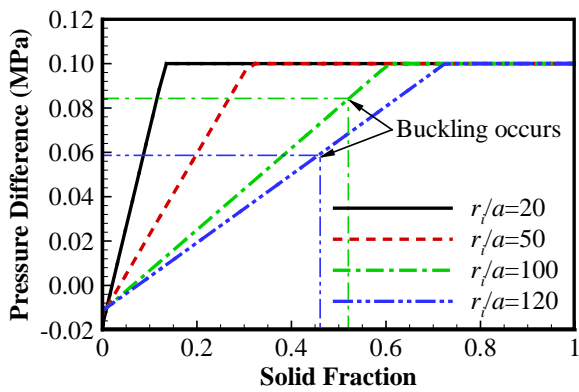


(c)

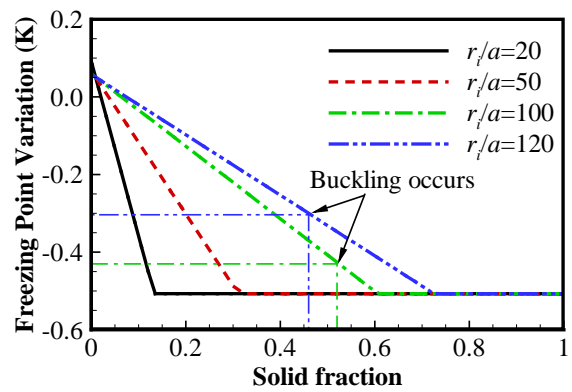


(d)

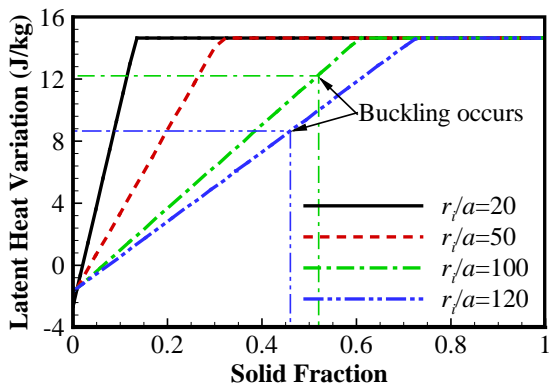
Fig. 3 Comparison with references: (a) Temperature profile at $t = 500$ s; (b) Solidification rate; (c) Pressure variation with solidification; (d) Variations of melting temperature and latent heat with solidification.



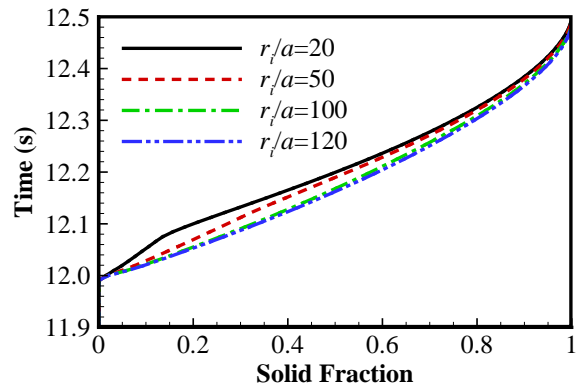
(a)



(b)



(c)



(d)

Fig. 4 Effects of shell thickness during solidification: (a) Evolution of pressure differences; (b) Evolution of freezing point variation; (c) Evolution of latent heat variation; (d) Time with respect to solid fraction. Critical position of buckling is labelled.

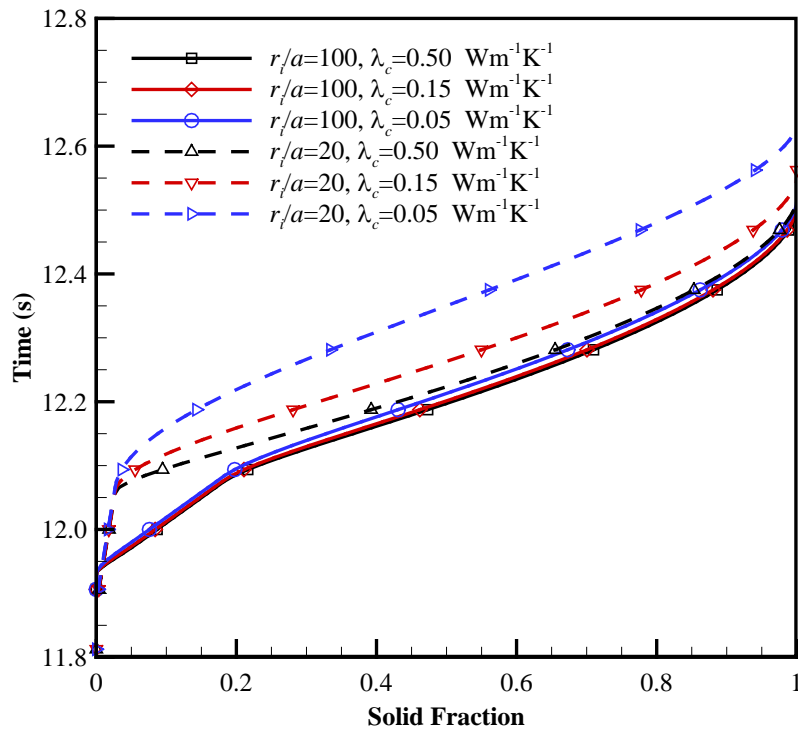


Fig. 5 Effect of shell thickness with different thermal conductivities on solidification time.

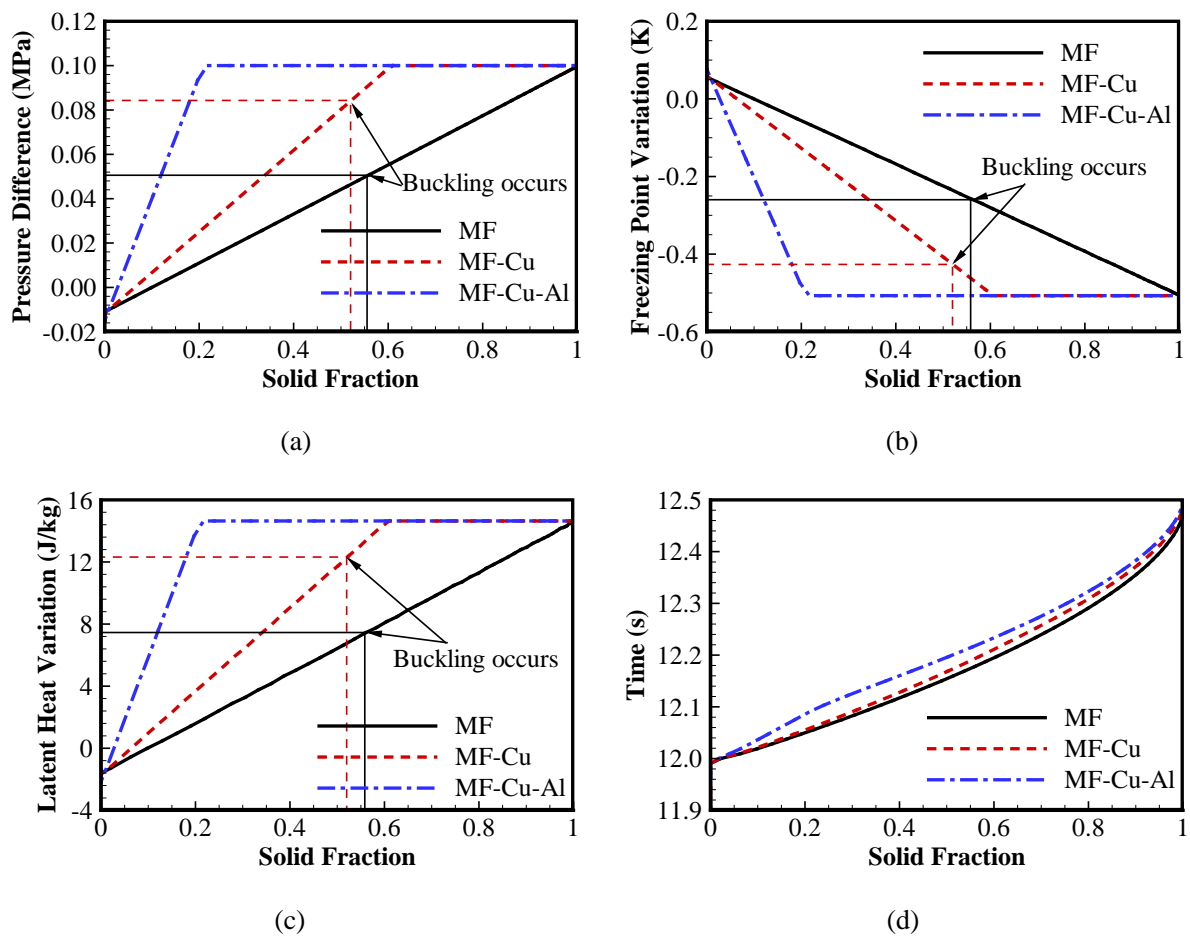
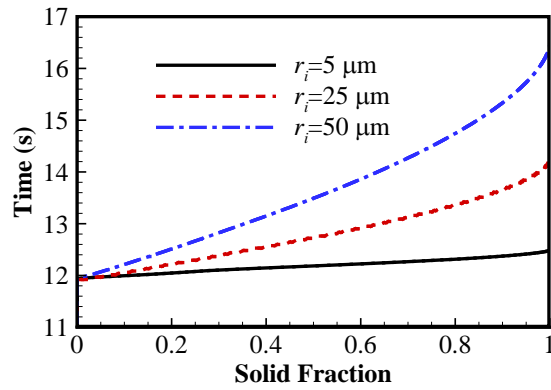
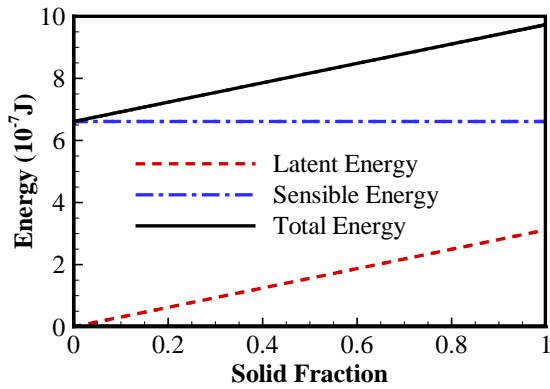


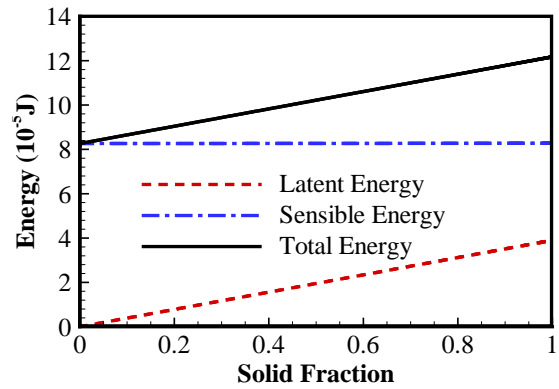
Fig. 6 Effects of shell compositions during solidification: (a) Evolution of difference pressures; (b) Evolution of freezing point variation; (c) Evolution of latent heat variation; (d) Time with respect to solid fraction. Critical position of buckling is labelled.



(a)



(b)



(c)

Fig. 7 Effects of microcapsule size during solidification: (a) Time with respect to solid fraction; (b,c) Evolution of the stored energy at $r_i = 5 \mu\text{m}$ and $25 \mu\text{m}$.

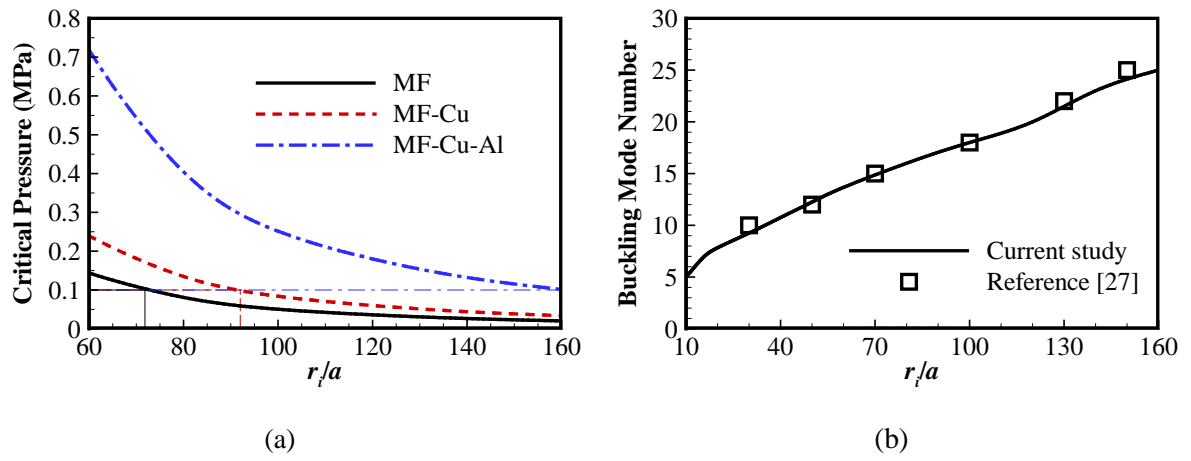


Fig. 8 (a) Critical buckling pressure with respect to r_i/a for different shell compositions; (b) Buckling mode numbers with respect to r_i/a .

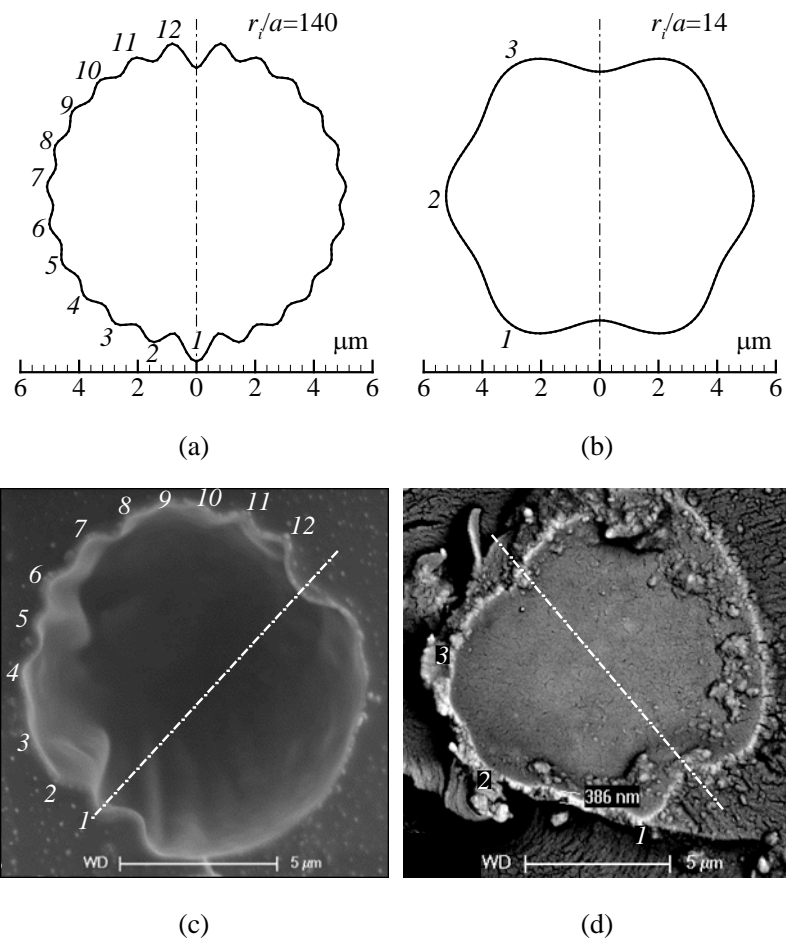


Fig. 9 Calculated buckling modes at $r_i/a= 140$ (a) and 14 (b); Cross-sectional images of buckling MF-Cu microcapsules under Cryo-SEM (c) and TEM (d). The waves are partially labeled with numbers and the dot-dash line represents symmetry axis. The buckling on one side of symmetry axis vanished when the microcapsules were cut.

Table 1 Properties of DJ used in simulations [42].

	Properties	Symbol	Value	Unit
DJ in liquid state	Density	ρ_{l0}	931.3	$\text{kg}\cdot\text{m}^{-3}$
	Specific heat	c_{pl}	1584	$\text{J}\cdot\text{kg}^{-1}\cdot\text{K}^{-1}$
	Compressibility	β_l	1.72×10^{-10}	Pa^{-1}
	Thermal expansion	α_l	8.33×10^{-4}	K^{-1}
	Thermal conductivity	λ_l	0.148	$\text{W}\cdot\text{m}^{-1}\cdot\text{K}^{-1}$
	Surface tension	γ_l	0.028	$\text{N}\cdot\text{m}^{-1}$
DJ in solid state	Density	ρ_{s0}	950.0	$\text{kg}\cdot\text{m}^{-3}$
	Specific heat	c_{ps}	1500	$\text{J}\cdot\text{kg}^{-1}\cdot\text{K}^{-1}$
	Compressibility	c_{ps}	0	Pa^{-1}
	Thermal expansion	α_s	0	K^{-1}
	Thermal conductivity	λ_s	0.152	$\text{W}\cdot\text{m}^{-1}\cdot\text{K}^{-1}$
L \leftrightarrow S	Freezing temperature at P_0	T_{f0}	-81	$^{\circ}\text{C}$
	Latent heat at (T_{f0}, P_0)	L_{f0}	80	$\text{kJ}\cdot\text{kg}^{-1}$

Table 2 Theoretical properties of MF [43].

Properties	Symbol	Value	Unit
Density	ρ_c	1500	$\text{kg}\cdot\text{m}^{-3}$
Specific heat	c_{pc}	1200	$\text{J}\cdot\text{kg}^{-1}\cdot\text{K}^{-1}$
Thermal expansion	α_c	6.0×10^{-5}	K^{-1}
Thermal conductivity	λ_c	0.5	$\text{W}\cdot\text{m}^{-1}\cdot\text{K}^{-1}$
Young's modulus	E_c	7.0×10^9	Pa
Poisson's ratio	ν_c	0.29	--

Table 3 Comparison of energy storage capacity between a typical packed bed and the MEPCMS for PTES and LAES. The storage materials are Fe_3O_4 (density 5175 kg/m^3) and quartzite (density 2560 kg/m^3) in the packed beds for PTES and LAES systems, respectively. The carrier liquids are R22 and propane in the MEPCMSs for PTES and LAES systems, respectively.

	Unit	Packed bed (PTES)	MEPCMS (PTES)	Packed bed (LAES)	MEPCMS (LAES)
Pressure	bar	1.05	1.05	1.49	1.49
Temperature range	K	123~223	123~223	92.7~192.7	92.7~192.7
Void fraction	--	0.35	--	0.38	--
Average specific heat	$\text{J}\cdot\text{kg}^{-1}\cdot\text{k}^{-1}$	520	1125	541	1861
Equivalent latent heat	$\text{kJ}\cdot\text{kg}^{-1}$	--	11.1	--	21.8
Mass-based energy storage density	$\text{kJ}\cdot\text{kg}^{-1}$	52.0	123.6	54.1	207.9
Volume-based energy storage density	$\text{MJ}\cdot\text{m}^{-3}$	174.9	180.1	85.9	154.1